Journal of Alloys and Compounds 489 (2010) 183–187

Contents lists available at ScienceDirect

Journal of Alloys and Compounds

journal homepage: www.elsevier.com/locate/jallcom

Multiple maxima in glass-forming ability in Al–Zr–Ni system

H. Yang, K.Y. Lim, Y. Li *

Department of Materials Science and Engineering, Faculty of Engineering, National University of Singapore, Singapore 117576, Singapore

ARTICLE INFO

Article history:
Received 11 May 2009
Received in revised form 8 September 2009
Accepted 9 September 2009
Available online 16 September 2009

Keywords:
Metallic glasses
Glass-forming ability
Rapid-solidification

ABSTRACT

In this paper, we report one interesting finding of a multiple maxima in glass-forming ability within a single eutectic system in the Al-rich region of Al–Zr–Ni ternary alloys. This is the first time that two local optimum glass formers in a single eutectic system have been reported. It is hereby suggested that glass formation is an intricate balance of kinetic, thermodynamic and topological factors.

1. Introduction

After some three decades of frenzy in discovering new metallic glasses (MGs) in metallic alloy systems, following the ground-breaking report in the Au–Si [1] system, the search for MGs in Al-rich systems were thwarted over and over again. Finally by virtue of the independent work of Inoue et al. [2,3] and He et al. [4], Al-rich alloys containing RE (where RE = Y or Lanthanide element) and LTM (where LTM = Ni, Co, Fe or Cu), were melt spun into monolithic glassy phase. Since then, Al-based metallic glasses with high Al content have attracted considerable interest as a result of a combination of high strength, specific strength and good bending ductility. More recently, Al-based bulk metallic glasses (BMGs) with critical size up to 1 mm were reported independently by several research groups [5,6]. However, in comparison with other metal-based BMGs, Al-based alloys still exhibit poorer glass-forming ability and have thus been labeled as "marginal glass former(s)" [7].

Presently, the search for Al-based MGs or BMGs was predominantly centered on Al–LTM–RE alloys [8–20]. However, one group of alloys which has been overlooked is that of the Al–ETM–LTM alloy system (where ETM = Zr, Hf or Ti), most notably the Al–Zr–Ni alloy system. The glass formation in this alloy system is well worth studying as the constituent elements also have large atomic size mismatch and negative mixing enthalpy of each atomic pairs. These factors theoretically should make the atomic packing more dense, retard diffusion, and inhibit crystallization in the super-cooled liquid, thereby increasing the alloy's relative ease for glass formation.

In this paper, we present the results of our GFA study in the Al-rich corner of the Al–Zr–Ni alloy system. Two distinct peaks in GFA, which were clearly separated by regions of very poor GFA, were located by carefully studying the GFA of the alloys in this region. Interestingly, these two peaks appear to belong to the same eutectic system, contrary to the notion that only one best glass former or best glass-forming zone could be found in each eutectic system [21,22]. The reason for the multiple maxima in glass formation will be explained by considering topological, kinetic and thermodynamics factors.

2. Experimental

Pure elements of Al (99.9%), Ni (99.98%) and Zr (>99.5%) were arc-melted in a Ti-gettered purified Ar atmosphere. Each ingot was re-melted at least 5 times to ensure chemical homogeneity. The ingots were then induction melted in a quartz tube in a purified Ar atmosphere, the molten alloys were then melt spun at a rotating copper wheel speed of 30 or 40 m s^{-1}. Melt spun ribbons so produced had typical widths of 2–3 mm, and thicknesses of 20–40 μm. Differential scanning calorimetry (DSC) runs were carried out at 20 K min^{-1} up to a temperature of 873 K, under 70 ml min^{-1} constant Ar gas flow. Melting studies were carried out at 10 K min^{-1} up to 1673 K. X-ray diffraction (XRD) patterns were obtained using Cu Kα radiation.

In our study, alloy ingots of compositions with promising GFA were induction re-melted in a quartz tube in a purified Ar atmosphere. The molten alloy was then injected into a wedge shaped cavity in a copper mould at a net Ar pressure of ~1.5 bar. The critical thickness for full glass formation was defined by a conspicuous curved delineation spanning across the wedge cast ingot, denoted hereafter as t_{amor}. This method has been reported by Sanders et al. [12] to obtain fully amorphous ingots of the alloy $Al_{86}La_5Ni_9$ with ~780 μm in thickness. Our wedge cast ingots were sectioned, mounted on its side and set in resin. The longitudinal section was grinded and polished, and etched by using a modified Keller's reagent (5 ml HNO_3, 3 ml HCl, 2 ml HF and 250 ml distilled water). Micrographs were obtained typically using scanning electron microscopy (SEM).

* Corresponding author. Tel.: +65 6516 3348; fax: +65 6776 3604.
E-mail address: mseliy@nus.edu.sg (Y. Li).

0925-8388/$ – see front matter © 2009 Elsevier B.V. All rights reserved.
doi:10.1016/j.jallcom.2009.09.049

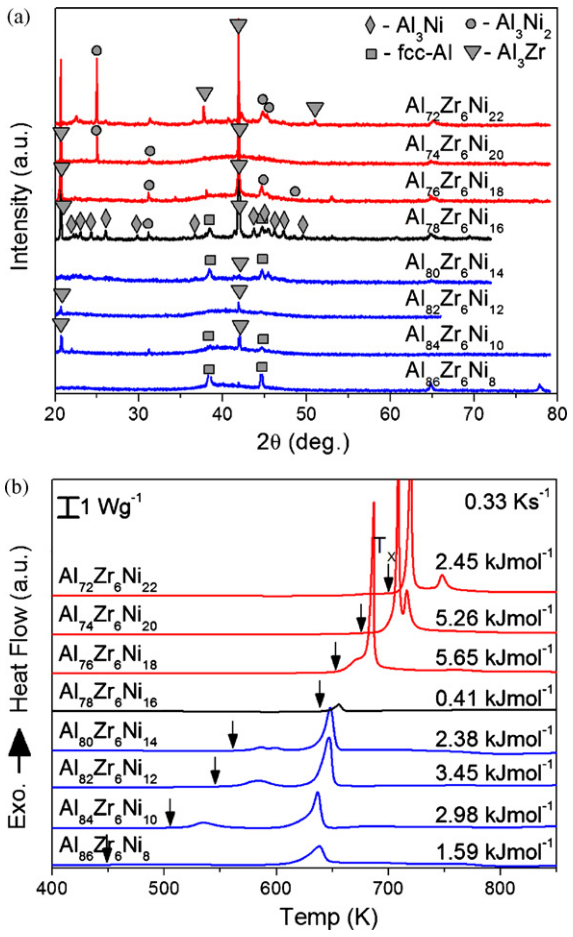

Fig. 1. (a) XRD patterns and (b) DSC traces of the alloy series $Al_{94-x}Zr_6Ni_x$ (x = 8–22 at.%, at 2 at.% interval), showing two amorphous forming regions truncated by the alloy at $Al_{78}Zr_6Ni_{16}$.

3. Results

Fig. 1a shows the XRD patterns of the series of as-spun alloys, $Al_{94-x}Zr_6Ni_x$ (x = 8–22 at.% at 2 at.% interval), where the Zr content was fixed at 6 at.% and the Ni content increased at the expense of Al, and Fig. 1b shows the corresponding DSC curves. An interesting trend is apparent from the XRD pattern and DSC curves of this series of alloys. There are obviously *two* amorphous forming region segregated by the composition $Al_{78}Zr_6Ni_{16}$, which is fully crystalline. The first, which lies between $Al_{86}Zr_6Ni_8$ and $Al_{80}Zr_6Ni_{14}$, is Al-enriched, and the amorphous phase of these alloys shows relatively lower thermal stability. The second amorphous forming region however, is solute enriched, which lent thermal stability to the amorphous phase.

By careful study of the GFA of the alloys at a small composition interval in the amorphous forming region with high solute content, we were able to locate the best amorphous forming alloy at the composition $Al_{75.5}Zr_{5.5}Ni_{19}$. Fig. 2a shows the XRD patterns of this alloy and two others adjacent to it, and Fig. 2b shows the corresponding DSC traces. The heat of crystallization as shown in Fig. 2b clearly peaks at the alloy $Al_{75.5}Zr_{5.5}Ni_{19}$ with a value of ΔH_X = 5.74 kJ mol^{-1}, indicating higher amorphous content compared to its adjacent alloys. The XRD pattern for this alloy shows a symmetrical broad hump with no trace of a crystalline peak. On the other hand, XRD patterns for both adjacent alloys showed some crystalline phases, and can be identified as fcc-Al in the alloy $Al_{77}Zr_5Ni_{18}$; and Al_3Zr and Al_3Ni_2 for the alloy $Al_{74}Zr_6Ni_{20}$. Under

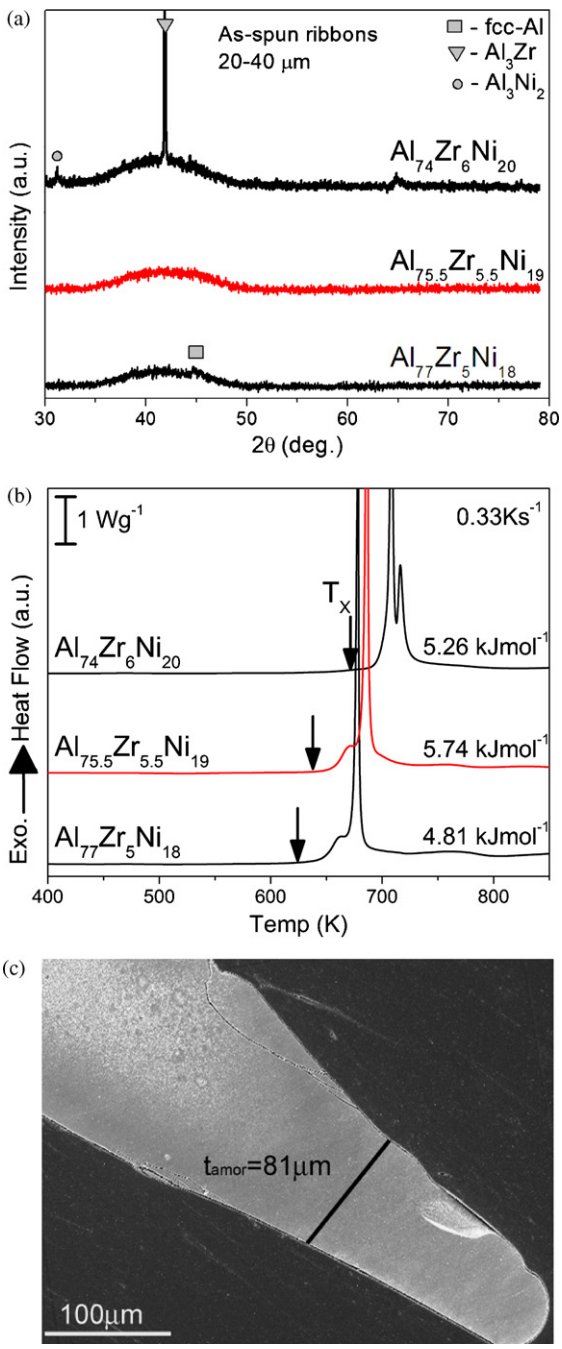

Fig. 2. (a) XRD patterns, and (b) DSC traces of $Al_{75.5}Zr_{5.5}Ni_{19}$ and two adjacent alloys: $Al_{77}Zr_5Ni_{18}$ and $Al_{74}Zr_6Ni_{20}$ and (c) SEM micrograph of wedge cast ingot of the alloy $Al_{75.5}Zr_{5.5}Ni_{19}$.

wedge casting condition, the critical size for amorphous formation for alloy $Al_{75.5}Zr_{5.5}Ni_{19}$ was approximately 81 μm (Fig. 2c).

Similarly, by carefully studying the GFA of the alloys in the lower solute content region, we were able to locate the best amorphous forming alloy near the composition $Al_{82}Zr_5Ni_{13}$. Fig. 3a shows the XRD patterns of the alloy $Al_{82}Zr_5Ni_{13}$ and two others adjacent to it, and Fig. 3b shows the corresponding DSC traces. The heat of crystallization as shown in Fig. 2b is the highest for the alloy $Al_{82}Zr_5Ni_{13}$ with a value of ΔH_X = 3.24 kJ mol^{-1}, indicating higher amorphous content compared to its adjacent alloys. The XRD pattern for this alloy shows a broad hump with no trace of a crystalline peak. On the other hand, XRD patterns for both adjacent alloys showed some crystalline phases, and can be attributed to fcc-Al. Wedge casting

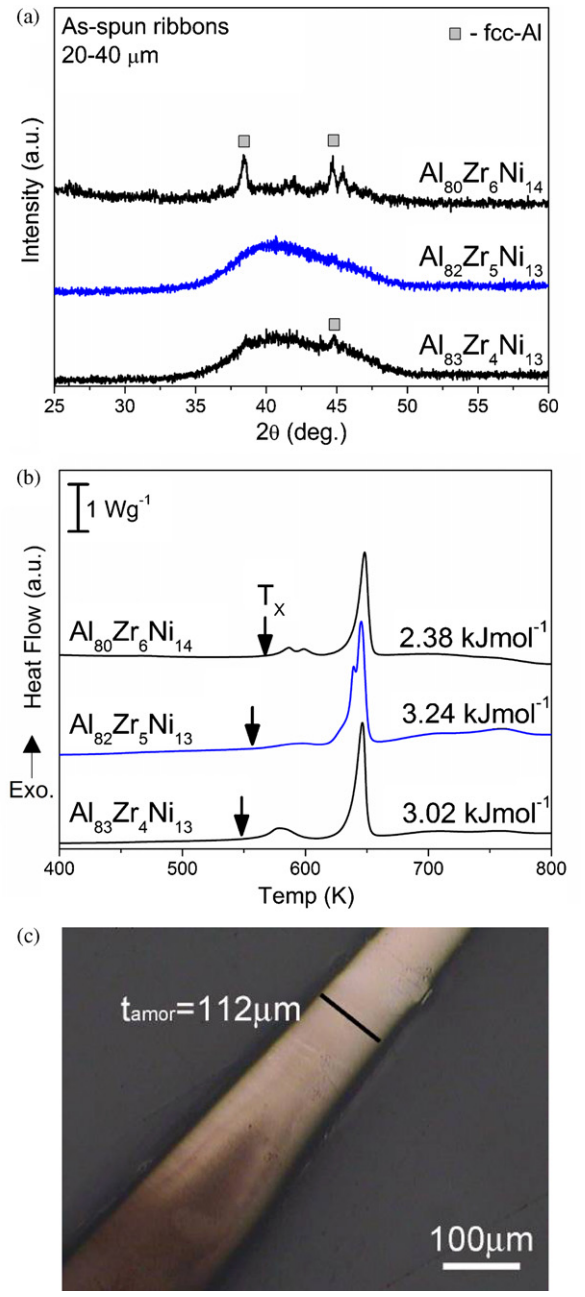

Fig. 3. (a) XRD patterns, (b) DSC traces of $Al_{82}Zr_5Ni_{13}$ and two adjacent alloys: $Al_{83}Zr_4Ni_{13}$ and $Al_{80}Zr_6Ni_{14}$ and (c) optical micrograph of wedge cast ingot of the alloy $Al_{82}Zr_5Ni_{13}$.

revealed that the critical size for amorphous formation for alloy $Al_{82}Zr_5Ni_{13}$ was approximately 112 μm (Fig. 3c).

We have also conducted studies on the melting behavior of this series of alloys, as well as the two optimal amorphous forming alloys. The solidus and liquidus temperatures of the samples were extracted and plotted in Fig. 4 as a function of the total solute content, taken to be the sum of the Zr and Ni content in the alloy. Interestingly, regardless of the solute content, all of the samples commence melting at almost the same temperature of 907–909 K. Furthermore, liquidus temperature progressively rises with increasing solute content. This hinted that all of these alloys, notably our two optimum amorphous alloys, despite significant differences in the solute content, are related to the same eutectic reaction.

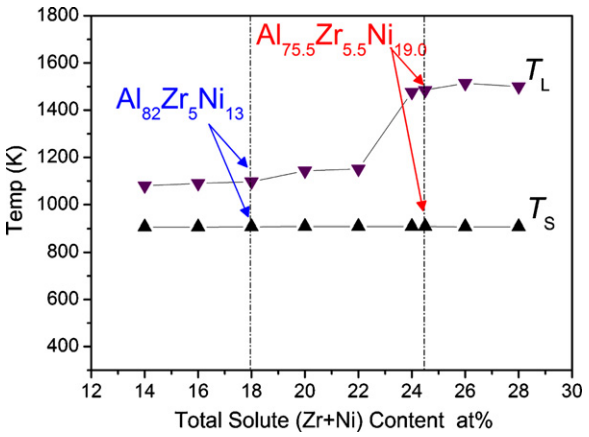

Fig. 4. Liquidus, T_L, and solidus, T_m, temperatures plotted as function of the total solute (Zr + Ni) content. All alloys commence melting at a same temperature.

In summary, our study has revealed the existence of multiple peaks in GFA in our current alloy system. One is at $Al_{75.5}Zr_{5.5}Ni_{19}$ with a critical size of 81 μm, and another is at $Al_{82}Zr_5Ni_{13}$ with a critical size of 112 μm. These two peaks were clearly truncated from regions of very poor GFA, represented by the alloy of $Al_{78}Zr_6Ni_{16}$. In addition, these two alloys probably belong to the same eutectic system, despite the large difference in solute content.

This work is the first time that the local peak(s) in GFA in a single eutectic system has been carefully studied and the critical size for fully amorphous formation for each of these two alloys has been reported. Furthermore, both of our alloys were Ni enriched, similar to a recent work in Al–RE–Ni by Yang et al. [17], unlike many other Al-based MGs which were often Ni-poor [2,3].

4. Discussion

4.1. On the predictive capability of Miracle's efficient cluster packing model

Recently, Miracle has proposed the efficient cluster packing (ECP) [23–25] model which places an overriding importance on the atomic size of the species in a multi-component metallic glass former. In this structural model, α-solute-centric clusters with Ω-solvent atoms only in the first coordination shell can maximize space filling by adopting an fcc, hcp, bcc or sc packing of the clusters. In the midst of these clusters are octahedral and tetrahedral interstices which are occupied by β- and γ-solutes, respectively. For each type of cluster packing, the α-, β-, γ- and Ω-sites can be easily deduced, this model thus provide for a "user-friendly" platform to predict the glass-forming compositions.

Table 1 illustrates Miracle's ECP model employed on the alloy system, Al–Zr–Ni, studied in this work. Unfortunately it is clear that none of the predicted compositions could match the actual optimum amorphous formers in our study. In fact, evidence from

Table 1
Predicted alloy compositions for glass formation in the Al–Zr–Ni alloy system using Miracle's ECP Model.

Alloy system:		Al–Zr–Ni		
ECP structure:		$\langle 15,12\rangle_{fcc}$		
Site occupancy				
α-sites	Ω-sites	β-sites	γ-sites	Predicted composition
1	8.3	1	0	$Al_{80.64}Zr_{9.68}Ni_{9.68}$
1	8.3	1	1	$Al_{73.53}Zr_{8.82}Ni_{17.65}$
1	8.3	1	2	$Al_{67.57}Zr_{8.11}Ni_{24.32}$

Table 2
Correlation of ratios between constituent atom pairs in the optimum glass-forming alloys and their critical size for full glass formation.

Best glass former	Ni:Zr ratio	Al:Ni ratio	Al:Zr ratio	Critical size (μm)
$Al_{75.5}Zr_{5.5}Ni_{19.0}$	3.5	4.0	13.7	~81
$Al_{82.0}Zr_{5.0}Ni_{13.0}$	2.6	6.3	16.4	~112

XRD patterns and DSC traces (not shown here) of 20–40 μm thick as-spun ribbons of these predicted alloy compositions all showed that they were fully crystalline.

While it was claimed in his work that the model gave "very good agreement" between predicted and experimental observed alloy composition that can form glass for the Al–RE–LTM and Al–ETM–LTM glass-forming systems [24], we would prefer to regard the above predictive modeling as indicative of the *real* amorphous forming composition. Coupled with our empirical experience that GFA of glass formers are strongly composition dependent [26–28], the predicted composition of the model could serve as a powerful shortcut to locate the real best glass former in each alloy system. Despite this reservation, the structural model did drop us a hint that for a given alloy system, depending on the occupancy of the interstitial γ sites, there could be more than one composition capable of amorphous formation, which are located at compositions with discrete stoichiometric ratios between the primary and secondary solutes.

4.2. Enhanced GFA due to the formation of densely packed solute-centric clusters

While examining the Zr to Ni ratio of the two best amorphous formers, we noticed an interesting trend in the Al to Ni ratio, and the Al to Zr ratio and its correlation with the critical sizes for fully amorphous formation. Table 2 summarizes these observations for these two alloys.

As illustrated in the table, the ratio of Al to Ni for $Al_{75.5}Zr_{5.5}Ni_{19}$ is ~4. This would suggest that on average, each Ni atom is coordinated by four Al atoms, forming a Ni-centric tetrahedron. This coordination is quite consistent with that of the tetrahedral γ sites. On the other hand, the Al to Ni ratio for $Al_{82}Zr_5Ni_{13,}$ is ~6.3, which would suggest an octahedron involving Ni atoms coordinated by six Al atoms. This coordination is consistent with that of the octahedral β sites. Since we know that a six-coordinated octahedron has a higher packing efficiency than that of a four-coordinated tetrahedron and coupled with the observation that the coordination of Al atoms around Zr in the amorphous alloy at $Al_{82}Zr_5Ni_{13}$ is also significantly higher, we should expect a denser packing of atoms that can more effectively retard crystallization and thus vitrify more readily. The larger critical size for the alloy $Al_{82}Zr_5Ni_{13}$ has affirmed this correlation between the GFA of an alloy and the formation of efficiently and densely packed solute-centric clusters.

4.3. Kinetics and thermodynamics considerations for the existence of multiple maxima in GFA

The eutectic composition has conventionally played a pivotal role in determining the optimum glass former in a given alloy system. Classically, it was believed that a high reduced glass transition of above 2/3 can effectively suppress the nucleation necessary for crystallization [29], leading to easier glass formation. Assuming that the glass transition temperature is only weakly dependent on composition, while the liquidus temperature is the lowest at the eutectic composition, the eutectic point naturally has the highest T_{rg}, and thus would potentially have the highest GFA.

Recently, Li and co-workers [21,30] have extended classical solidification theory to metallic glass, and argued that the suppression of further growth of the nuclei, could also lead to easy glass formation, as long as the glass transition temperature, T_g exceeds the interface temperature of all other competing phases, in the alloy system. Yet, either Turnbull's or Li's kinetic considerations are centered on a eutectic alloy or eutectic coupled zone which is unique for each eutectic system. Therefore, for any eutectic system, there should only be a single best glass former or best glass-forming zone, either symmetrically or asymmetrically, located about the eutectic composition. The existence of two separate local peaks in glass formation in our alloy system is difficult to explain from a kinetic standpoint alone, especially since both alloys appeared to undergo the same eutectic reaction.

Thermodynamically, easy glass formers with low critical cooling rates have a low driving force for crystallization, as there is a small difference in Gibbs free energy between the supercooled liquid and its crystalline counterpart. The small difference in Gibbs free energy is a result of large entropy of fusion, in the case of multi-component alloys; and high value of T_{rg} [31]. Clearly, thermodynamics aspects of glass formation is also closely related to the eutectic and is a singular event: for a multi-component alloy system, the composition at which there is the lowest energy difference between the liquid and solid phase, would give the best glass former. Again, thermodynamic consideration alone could not explain our observed results of two maxima in GFA in a single eutectic system.

We have discussed the existence of the multiple maxima in GFA in a single eutectic system in this alloy system, from topological, kinetic and thermodynamic considerations. It is apparent that, when taken alone, none of the factors seemed to be able to fully explain this phenomenon we have observed. It is suggested that glass formation is an intricate balance of kinetic, thermodynamic and also topological factors. Perhaps in good glass formers, all factors could come to a consensus at one composition or one compositional zone, where the best glass former(s) are located. However, for marginal glass formers like Al-based alloys, each of these factors could point to a different alloy composition, where conditions are best suited for glass formation.

5. Conclusions

In this work we have reported on the observation of two local peaks in GFA, in a single eutectic system in the Al-rich corner of an Al–Zr–Ni alloy system. The maxima were located at $Al_{75.5}Zr_{5.5}Ni_{19}$, whose critical size was approximately 81 μm, and another at $Al_{82}Zr_5Ni_{13}$, whose critical size was approximately 112 μm. To the best of our knowledge, this is the first time that the local peaks in GFA have been carefully studied and the critical size for fully amorphous formation for each of these two alloys has been reported.

The glass formation in this alloy system was discussed from topological, kinetics and thermodynamics considerations. Actual topology deduced from the alloy compositions was found to deviate from the predicted topology based on Miracle's ECP model. Despite its inadequacy in accurately predicting the optimum glass-forming compositions, the model does provide a hint of multiple peaks in GFA depending on the occupancy of the interstitial sites by the solutes. Kinetic and thermodynamic considerations are both centered on the eutectic composition or eutectic coupled zone, which is unique to each alloy system. Therefore the factors that favor easiest glass formation should also point to just one best glass former or best glass-forming zone in a single eutectic system. Taken independently, none of the factors could fully explain the experimentally observed multiple peaks in GFA in a single eutectic system in our current alloy system. It is hereby suggested that glass formation is an intricate balance of kinetic, thermodynamic and topological factors as well. For marginal glass formers like Al-based MGs, each of these factors could point to a different alloy composition, where conditions are best suited for glass formation.

Acknowledgements

This work was supported by the MINDEF-NUS Joint Applied R&D Cooperative Program Project, Grant No. R284-000-041-123/232).

References

[1] W. Klement, R.H. Willens, P. Duwez, Nature 187 (1960) 869.
[2] A. Inoue, K. Ohtera, K. Kita, T. Masumoto, Jpn. J. Appl. Phys. Part 2-Lett. 27 (1988) L1796–L1799.
[3] A. Inoue, K. Ohtera, A.P. Tsai, T. Masumoto, Jpn. J. Appl. Phys. Part 2-Lett. 27 (1988) L280–L282.
[4] Y. He, S.J. Poon, G.J. Shiflet, Science 241 (1988) 1640–1642.
[5] B.J. Yang, J.H. Yao, J. Zhang, H.W. Yang, J.Q. Wang, E. Ma, Scripta Mater. 61 (2009) 423–426.
[6] L.C. Zhuo, S.J. Pang, H. Wang, T. Zhang, Chin. Phys. Lett. (2009) 26.
[7] J.H. Perepezko, Prog. Mater. Sci. 49 (2004) 263–284.
[8] A. Inoue, Prog. Mater. Sci. 43 (1998) 365–520.
[9] J.H. Perepezko, R.J. Hebert, JOM-J. Min. Met. Mater. S. 54 (2002) 34–39.
[10] A. Inoue, N. Matsumoto, T. Masumoto, Mater. Trans. JIM 31 (1990) 493–500.
[11] F.Q. Guo, S.J. Poon, G.J. Shiflet, Mater. Sci. Forum 331–337 (2000) 31–42.
[12] W.S. Sanders, J.S. Warner, D.B. Miracle, Intermetallics 14 (2006) 348–351.
[13] A.K. Gangopadhyay, K.F. Kelton, Philos. Mag. A 80 (2000) 1193–1206.
[14] Z.C. Zhong, A.L. Greer, Int. J. Non-Equilib. Process. 11 (1998) 35–53.
[15] W.H. Jiang, M. Atzmon, Acta Mater. 51 (2003) 4095–4105.
[16] H.W. Yang, S.C. Tjong, J.Q. Wang, Mater. Sci. Eng. A 406 (2005) 160–165.
[17] H. Yang, J.Q. Wang, Y. Li, Philos. Mag. 87 (2007) 4211–4228.
[18] H. Yang, J.Q. Wang, Y. Li, J. Non-Cryst. Solids 354 (2008) 3473–3479.
[19] G.H. Li, W.M. Wang, X.F. Bian, J.T. Zhang, R. Li, L. Wang, J. Alloys Compd. 478 (2009) 745–749.
[20] H.W. Yang, W. Tong, X. Zhao, L. Zuo, J.Q. Wang, J. Alloys Compd. 473 (2009) 347–350.
[21] D. Wang, H. Tan, Y. Li, Acta Mater. 53 (2005) 2969–2979.
[22] C.L. Dai, H. Guo, Y. Li, J. Xu, J. Non-Cryst. Solids 354 (2008) 3659–3665.
[23] D.B. Miracle, Nat. Mater. 3 (2004) 697–702.
[24] D.B. Miracle, Acta Mater. 54 (2006) 4317–4336.
[25] D.B. Miracle, O.N. Senkov, J. Non-Cryst. Solids 319 (2003) 174–191.
[26] J. Zhang, H. Tan, Y.P. Feng, Y. Li, Scripta Mater. 53 (2005) 183–187.
[27] H. Tan, Y. Zhang, D. Ma, Y.P. Feng, Y. Li, Acta Mater. 51 (2003) 4551–4561.
[28] H. Yang, J.Q. Wang, Y. Li, J. Alloys Compd. 422 (2006) 86–91.
[29] D. Turnbull, Contemp. Phys. 10 (1969) 473–488.
[30] D. Ma, H. Tan, D. Wang, Y. Li, E. Ma, Appl. Phys. Lett. 86 (2005) 191906-1-3.
[31] R. Busch, Y.J. Kim, W.L. Johnson, J. Appl. Phys. 77 (1995) 4039–4043.